Embryonic Stem Cell Grafting in Normal and Infarcted Myocardium: Serial Assessment with MR Imaging and PET Dual Detection[1]

Hui Qiao, MD, PhD
Hualei Zhang, BS
Yuanjie Zheng, PhD
Datta E. Ponde, PhD
Dinggang Shen, PhD[2]
Fabao Gao, MD, PhD
Ashley B. Bakken, BA
Alexander Schmitz, PhD
Hank F. Kung, PhD
Victor A. Ferrari, MD
Rong Zhou, PhD

Purpose: To use magnetic resonance (MR) imaging and positron emission tomography (PET) dual detection of cardiac-grafted embryonic stem cells (ESCs) to examine *(a)* survival and proliferation of ESCs in normal and infarcted myocardium, *(b)* host macrophage versus grafted ESC contribution to serial MR imaging signal over time, and *(c)* cardiac function associated with the formation of grafts and whether improvement in cardiac function is related to cardiac differentiation of ESCs.

Materials and Methods: All animal procedures were approved by the institutional animal care and use committee. Murine ESCs were stably transfected with a mutant version of herpes simplex virus type 1 thymidine kinase, *HSV1-sr39tk*, and also were labeled with superparamagnetic iron oxide (SPIO) particles. Cells were injected directly in the border zone of the infarcted heart or in corresponding regions of normal hearts in athymic rats. PET and MR imaging were performed longitudinally for 4 weeks in the same animals.

Results: ESCs survived and underwent proliferation in the infarcted and normal hearts, as demonstrated by serial increases in 9-(4-[^{18}F]fluoro-3-hydroxymethylbutyl) guanine PET signals. In parallel, the hypointense areas on MR images at the injection sites decreased over time. Double staining for host macrophages and SPIO particles revealed that the majority of SPIO-containing cells were macrophages at week 4 after injection. Left ventricular ejection fraction increased in the ESC-treated rats but decreased in culture media–treated rats, and border-zone function was preserved in ESC-treated animals; however, cardiac differentiation of ESCs was less than 0.5%.

Conclusion: Dual-modality imaging permits complementary information in regard to cell survival and proliferation, graft formation, and effects on cardiac function.

Supplemental material: *http://radiology.rsnajnls.org/cgi/content/full/250/3/821/DC1*

[1] From the Departments of Radiology (H.Q., Y.Z., D.E.P., D.S., F.G., A.B.B., A.S., H.F.K., R.Z.), Bioengineering (H.Z.), and Medicine (Cardiovascular) (V.A.F.), University of Pennsylvania, B6 Blockley Hall, MC 6069, 422 Curie Blvd, Philadelphia, PA 19104. Received February 5, 2008; revision requested March 26; revision received June 17; accepted August 8; final version accepted August 27. R.Z. supported in part by a grant from the Pennsylvania Department of Health. The Pennsylvania Department of Health specifically disclaims responsibility for any analyses, interpretations, or conclusions. **Address correspondence to** R.Z. (e-mail: *zhou@rad.upenn.edu*).
[2] **Current address:** Department of Radiology and Biomedical Research Imaging Center, University of North Carolina at Chapel Hill, Chapel Hill, NC.

Radiology

Coronary heart disease accounts for 36% of all cardiovascular death and is the leading cause of heart failure in the United States (1). Although postinfarction survival rates have been improved, congestive heart failure caused by a large infarction or progressive unfavorable ventricular remodeling remains a major problem (2). Despite that cardiac transplantation is currently the most effective therapy, the disparity between organ demand and supply limits its applicability. A treatment strategy often referred to as "cellular cardiomyoplasty" is an attempt at cardiac repair through local (intramyocardial, intracoronary) or systemic (intravenous) delivery of a variety of cells, including fetal or neonatal cardiomyocytes, cardiac cells derived from adult atrial appendages, skeletal myoblasts, embryonic stem cells (ESCs), or bone marrow–derived mesenchymal and hematopoietic stem cells. The strategy is based on the potential of these cells to differentiate into cardiomyocytes to repopulate the damaged myocardium or to secrete cytokines (eg, growth factors) that promote the growth of existing cardiomyocytes and/or blood vessels in the border zone.

Monitoring the fate (eg, survival, differentiation, and distribution) of grafted cells noninvasively would permit investigation of factors that may enhance the survival and/or the cardiac differentiation of these cells. Reporter gene (3–5) and superparamagnetic iron oxide (SPIO)-based direct cell labeling approaches (6–12) have been used to track transplanted cells in the heart. However, the issue of whether the SPIO labels remain with the stem cells or are transferred to the scavenger cells has not been directly investigated because of the lack of a marker for cell survival. A combination of the two approaches would provide a true survival marker independent of SPIO labels in addition to a submillimeter magnetic resonance (MR) imaging description of cell distribution, integration of grafts with the myocardial wall, and changes of left ventricular (LV) function in response to graft formation. Therefore, we used MR imaging and positron emission tomography (PET) dual detection of cardiac-grafted embryonic stem cells (ESCs) (5,13) to examine *(a)* survival and proliferation of ESCs in normal and infarcted myocardium, *(b)* host macrophage versus grafted ESC contribution to serial MR imaging signal over time, and *(c)* cardiac function associated with the formation of grafts and whether improvement in cardiac function is related to cardiac differentiation of ESCs.

Advances in Knowledge

- Embryonic stem cells (ESCs) double labeled with a PET reporter gene and superparamagnetic iron oxide (SPIO) particles permit serial noninvasive evaluation of stem cell fate by using PET and MR imaging techniques.
- Direct injection of ESCs in border-zone myocardium improves left ventricular (LV) ejection fraction after myocardial infarction (MI) and preserves regional (border-zone) myocardial function.
- Grafting ESCs in either normal or infarcted hearts leads to teratoma formation, within which less than 0.5% of the cell population differentiated into cardiomyocytes.
- Most (94%) of the SPIO-containing cells in the graft are host macrophages at week 4 after injection.

Implications for Patient Care

- The ability to noninvasively track stem cell fate and to evaluate their effect on global and regional LV function may have a major effect on patient care and management.
- ESC-mediated improvements in LV function after MI seem unrelated to the low incidence of cardiac differentiation of ESCs.
- Because of the risk of teratoma formation, predifferentiated ESCs should be used for myocardial repair and potential clinical applications.
- The double-labeling approach should be translatable to study ESC-derived cardiac progenitor cells to refine strategies for stem cell–based treatments.

Materials and Methods

Double Labeling of ESCs with Herpes Simplex Virus Type 1 Thymidine Kinase Reporter Gene and SPIO Particles

Murine ESCs were stably transfected with *HSV1-sr39tk*, a mutant form of herpes simplex virus type 1 thymidine kinase, and were labeled with SPIO particles (Feridex; Berlex Laboratories, Montville, NJ). Details of stable transfection and SPIO labeling including compositions of labeling media, intracellular iron content, labeling efficiency, and cell viability are provided in Appendix E1 (*http://radiology.rsnajnls.org/cgi/content/full/250/3/821/DC1*).

Experimental Groups

All animal procedures were approved by the local institutional animal care and use committee. A total of 62 female athymic rats (age range, 7–9 weeks; weight range, 200–250 g) purchased from a supplier

Published online
10.1148/radiol.2503080205

Radiology 2009; 250:821–829

Abbreviations:
CNR = contrast-to-noise ratio
ESC = embryonic stem cell
ESV = end-systolic volume
FHBG = 9-(4-[^{18}F]fluoro-3-hydroxymethylbutyl) guanine
FS = fractional shortening
ID = injected dose
LV = left ventricle
MI = myocardial infarction
SPIO = superparamagnetic iron oxide

Author contributions:
Guarantors of integrity of entire study, H.Q., H.Z., Y.Z., R.Z.; study concepts/study design or data acquisition or data analysis/interpretation, all authors; manuscript drafting or manuscript revision for important intellectual content, all authors; manuscript final version approval, all authors; literature research, H.Q., D.S., R.Z.; experimental studies, H.Q., H.Z., Y.Z., D.E.P., D.S., F.G., A.S., R.Z.; statistical analysis, H.Q., H.Z., D.S., R.Z.; and manuscript editing, H.Q., H.Z., D.S., H.F.K., V.A.F., R.Z.

Funding:
This research was supported by the National Institutes of Health (grants R21EB 2473, R01-HL081185).

Authors stated no financial relationship to disclose.

(Frederick Cancer Center, Frederick, Md) were used in this study.

In a pilot study, 24 rats were used to determine the earliest time when in vivo PET signals from grafted cells could be detected in the heart (Appendix E1 [*http://radiology.rsnajnls.org/cgi/content/full/250/3/821/DC1*]). In the dual-modality imaging study, a total of 35 rats were used: eight in group 1, eight in group 2, and seven in group 3; four rats did not survive the surgery, and one died after imaging; seven failed to meet the specified range of infarct size. To evaluate for the presence of free SPIO particles and macrophage infiltration early after injection, an additional three rats (not infarcted) were injected with 1 million cells and were euthanized 4 hours later (Appendix E1 [*http://radiology.rsnajnls.org/cgi/content/full/250/3/821/DC1*]).

Myocardial Infarction and Transplantation of Double-labeled ESCs

The control group was composed of eight rats that did not undergo infarct surgery (group 1) and that received double-labeled cells: Four rats received 1 million cells and four rats received 5 million cells suspended in 50 and 100 μL Dulbecco's modified Eagle's medium, respectively, and the cells were injected at the mid-anterior wall.

Surgical procedures were performed in 27 rats to induce myocardial infarction (MI) by a physician with 7 years of experience in animal surgery, with 45-minute left anterior descending coronary artery ligation followed by reperfusion and intramyocardial injection of cells, according to a previously published protocol (14). If the rat survived and had an infarct size of 10%–30% LV volume estimated by using MR imaging, it was placed in group 2 or 3. Because multiple imaging sessions were required for each animal, a staggered scheme was used to achieve the targeted number of data sets. Two of the rats that had undergone surgery but did not have MI, as determined by using MR imaging, were used to provide the normal myocardial wall thickness. Rats in group 2 (n = 8) received double-labeled cells in the same surgical session as the infarct surgery. Four rats received 1 million cells and four rats received 5 million cells suspended in 50 and 100 μL Dulbecco's modified Eagle's medium, respectively, injected at the border along the pale (blanched) infarct region at the conclusion of the ligation period. Rats in group 3 (n = 7) were infarcted but received 100 μL Dulbecco's modified Eagle's medium without ESCs.

PET and MR Imaging

PET and MR imaging schedules are listed in Tables 1 and 2. To monitor the changes of SPIO signal over time, MR imaging was performed in group 1 at day 1 after injection and then weekly for 4 weeks. To compare ventricular function in ESC-treated and culture media–treated hearts, MR imaging was performed in groups 2 and 3 at day 1, at which time infarct size was also quantified, and at 4 weeks after surgery.

PET imaging was performed with a high-resolution (2-mm) dedicated small-animal PET scanner, which was based on a commercially manufactured unit (Mosaic; Philips Medical Systems, Cleveland, Ohio) (15,16). To delineate the myocardial wall, nitrogen 13 (^{13}N) ammonia (mean, 1.20 mCi ± 0.33 [standard deviation] [44.4 MBq ± 12.21] in 0.5 mL saline) was injected intravenously, followed by immediate data acquisition for 15 minutes. To facilitate direct fusion of ^{13}N-ammonia and 9-(4-[^{18}F]fluoro-3-hydroxymethylbutyl) guanine (FHBG) images, 30 minutes after injection of ammonia while the animal remained anesthetized, a mean of 1.34 mCi ± 0.50 (49.58 MBq ± 18.5) FHBG in 1 mL saline was injected; data acquisition started 1 hour later and lasted for 30 minutes.

MR imaging was performed with a 4.7-T horizontal bore magnet (Magnex Scientific, Walnut Creek, Calif) interfaced with a console (Inova; Varian, Palo Alto, Calif). To assess global function and SPIO-associated hypoenhancement, a T2*-weighted fast gradient-echo sequence (17) with a 20° flip angle, 3-msec echo time (to minimize cardiac motion), and effective repetition time equal to one heartbeat was

Table 1

PET Imaging Schedule in Groups 1 and 2

	Time 1*		Time 2†		Time 3†	
Factor	5 Million Cells	1 Million Cells	5 Million Cells	1 Million Cells	5 Million Cells	1 Million Cells
Days after injection‡	4–7	7–10	14–17	14–17	28–30	28–30

* The first time for detection of 1 and 5 million cells is set differently, because on the basis of the pilot study, the earliest time to detect 5 million cells in the heart was day 4 after injection, whereas the earliest time to detect 1 million cells was day 7 after injection (Appendix E1 [*http://radiology.rsnajnls.org/cgi/content/full/250/3/821/DC1*]).

† At the second and third times, PET was performed usually on 1 day, but could be 2 days, after MR imaging. The MR imaging schedules corresponding to these times are presented in Table 2.

‡ The window in the schedule is to accommodate nonavailability of tracer or PET scanner during the long-term experiment.

Table 2

MR Imaging Schedule

Group	Day 1	Week 1	Week 2	Week 3	Week 4
1	≤48 h	Days 6–8	Days 13–15	Day 21	Days 27–28
2	≤24 h	. . .	Days 13–15*	. . .	Day 27
3	≤24 h	. . .	. . .	. . .	Day 27

Note.—The data are the actual number of hours or days after cell injection when MR imaging was performed.

* Only those receiving 5 million cells in group 2 underwent MR imaging for coregistration at week 2.

used to acquire short-axis cine images with electrocardiographic and respiratory gating. The same sequence was set up for T1 weighting with a 60° flip angle and minimum echo time to acquire delayed hyperenhancement cine images (18,19) at 15–20 minutes after intravenous injection of 0.3 mmol/kg of gadodiamide (Omniscan; Nycomed, Princeton, NJ).

Analyses of PET and MR Images and Coregistration

PET images were analyzed to derive a tissue uptake index in percentage of injected dose (ID) per gram of heart tissue over time from groups 1 and 2. MR images were analyzed to evaluate the following parameters: *(a)* Hypointense area and contrast-to-noise ratio (CNR) at day 1 and week 4 were compared in group 1. *(b)* Infarct size was estimated by using delayed hyperenhancement images and was presented as the percentage of LV volume (18,19). *(c)* Global function, including end-diastolic volume, end-systolic volume (ESV), LV ejection fraction, and LV mass (which includes the mass formed by grafted ESCs [teratomas]) was determined. *(d)* Regional one-dimensional fractional shortening (FS) of the wall was measured at the anterior and posterior border-zone and septum (remote) regions in groups 2 and 3. Definition of these regions is provided in Appendix E1 (*http://radiology.rsnajnls.org/cgi/content/full/250/3/821/DC1*), as are details of PET and MR image analyses and coregistration.

Immunohistochemical Staining of Macrophages, SPIO, Scars, and Teratoma

All animals were euthanized at week 4. Immunohistochemical staining was performed for the following analyses: *(a)* To

Figure 1

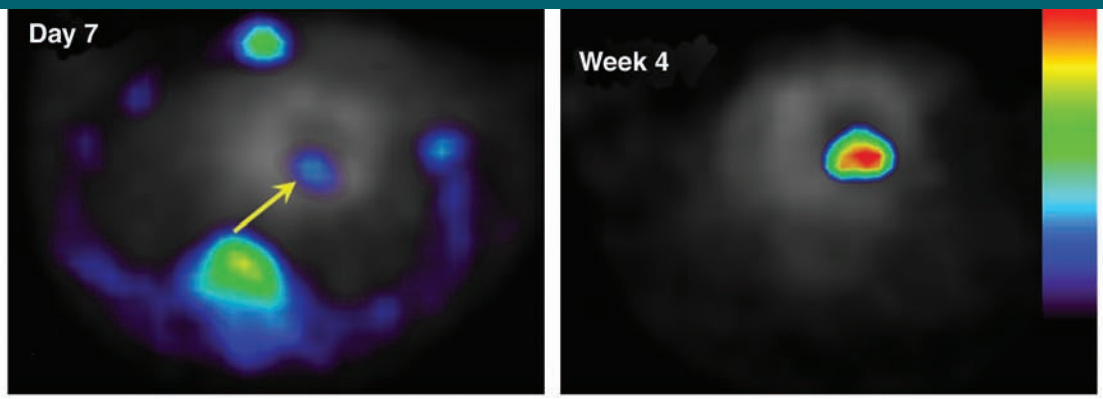

Figure 1: Detection of double-labeled ESCs by using FHBG PET via reporter gene expression. Intramyocardial location of FHBG signal of 5 million cells injected in normal heart is demonstrated by overlay of FHBG (color) and ^{13}N-ammonia images (gray scale) in axial view. **(a)** Day 7 and **(b)** week 4 after injection. Over time, when FHBG signal from cardiac regions became stronger, nonspecific FHBG signal was suppressed. Figure E4 (*http://radiology.rsnajnls.org/cgi/content/full/250/3/821/DC1*) shows three orthogonal views of heart.

Figure 2

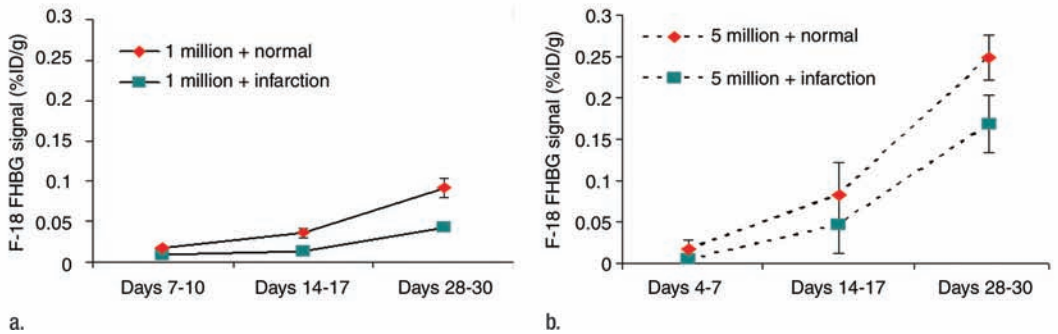

Figure 2: Time course of FHBG signal intensity in percentage ID per gram for **(a)** 1 million cells and **(b)** 5 million cells grafted in normal and infarcted hearts. At days 28–30, percentage of ID per gram from rats receiving 5 million cells was significantly stronger than those receiving 1 million cells in normal (mean, 0.249 ± 0.027 vs 0.092 ± 0.012; $P < .05$) and infarcted (mean, 0.169 ± 0.035 vs 0.043 ± 0.002; $P < .05$) hearts.

Figure 3

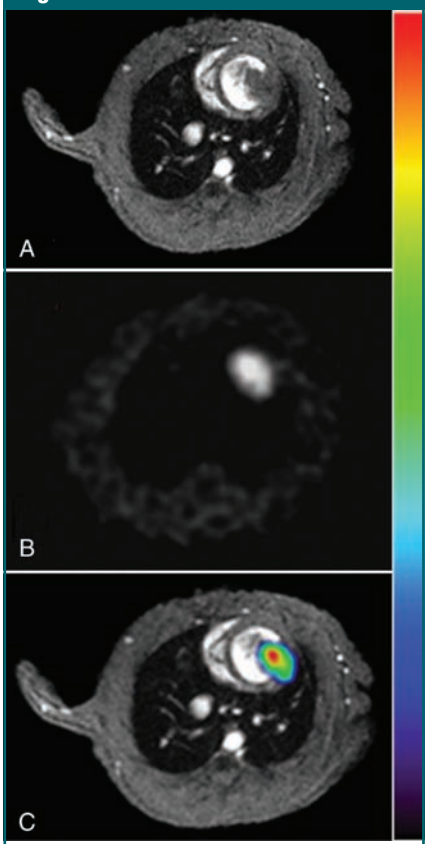

Figure 3: Coregistration of PET and MR images. *A,* Short-axis cardiac MR image (section 4 from multisection series) of infarcted heart 14 days after receiving 5 million double-labeled ESCs. *B,* Corresponding FHBG image. *C,* Coregistered color-scale PET images and gray-scale MR images obtained by using mutual-information–based algorithm. Figure E5 (*http://radiology.rsnajnls.org/cgi/content/full/250/3/821/DC1*) shows coregistration of multiple short-axis sections.

Figure 4

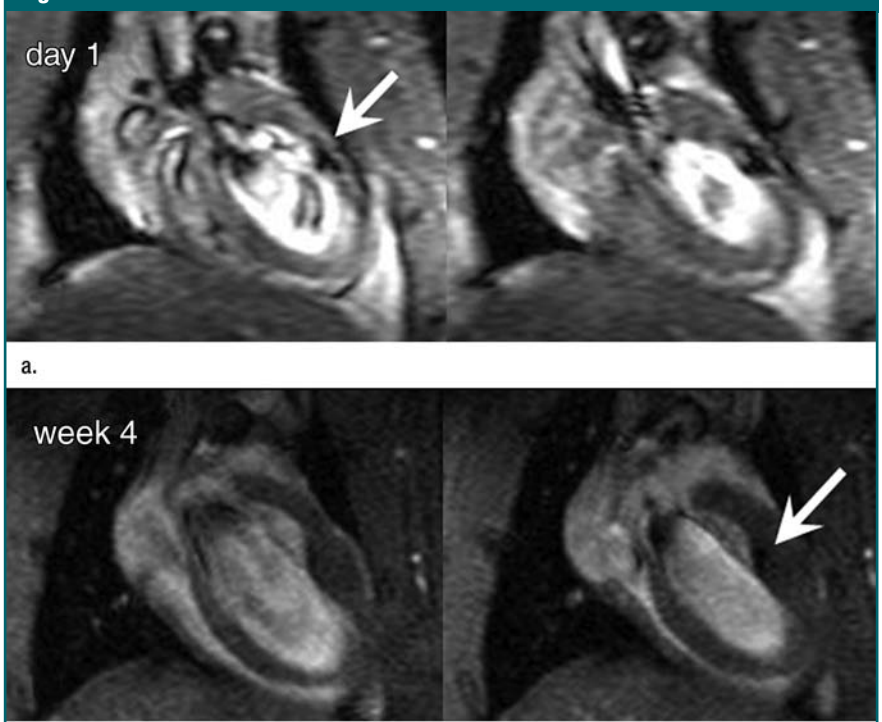

Figure 4: MR imaging detection of double-labeled ESCs. Two diastolic phases from cine long-axis images at **(a)** day 1 and **(b)** week 4 after injection of 1 million ESCs. Arrow = SPIO-associated hypointense region.

Figure 5

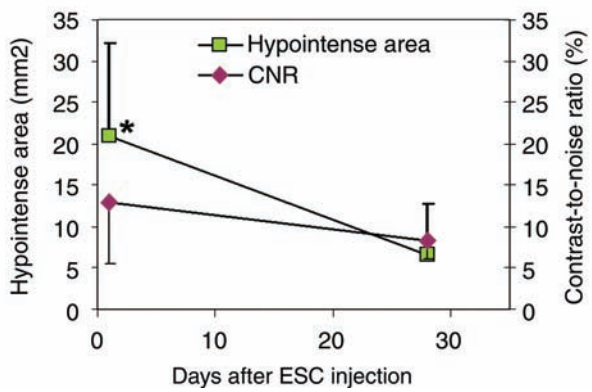

Figure 5: Changes of hypointense area and CNR over time on MR images. Hypointense area measured from group 1 rats decreased significantly at week 4 compared with measurement at day 1, whereas decrease of CNR was not significant. * = $P < .05$ between day 1 and week 4.

confirm the location of the grafts (teratoma) relative to the infarcted region, Masson trichrome staining (20) was performed to identify the fibrotic scar tissues. *(b)* Cardiac differentiation of ESCs in the grafts was evaluated by immunostaining of cardiac-specific sarcomeric α-actinin. *(c)* The location of SPIO particles at week 4 and their association with macrophages were examined by using double staining for macrophages (CD68) and SPIO particles.

Statistical Analysis

Data were presented as the mean ± standard deviation and were analyzed with software (SigmaStat; SPSS, Chicago, Ill). Changes of global and regional function were compared between groups 2 and 3; percentage of ID per gram and percentage of cardiomyocytes in the grafts (teratoma) were compared between 1 million and 5 million cell doses in groups 1 and 2; changes in hypointense area and CNR

were compared between day 1 and week 4 in group 1. A Mann-Whitney rank-sum analysis test was performed when the two groups were compared, whereas a one-way analysis of variance was used when more than two groups were compared. A difference with a *P* value of less than .05 was considered to be significant.

Table 3

Changes in Global Cardiac Function over 4 Weeks

Treatment Group	ΔEDV (μl)	ΔESV (μl)	ΔLV Ejection Fraction (%)	ΔLV Mass (mg)	ΔHeart Rate (beats/min)
Group 2 ($n = 8$)	60 ± 43	−14 ± 7	12 ± 8	264 ± 26	−58 ± 23
Group 3 ($n = 7$)	138 ± 44	117 ± 80	−15 ± 15	−16 ± 93	−32 ± 42
P value	<.05	<.03	<.02	<.001	NS

Note.—For each parameter, change was measured by subtracting value at day 1 from value at week 4. *P* values represent a significant difference except where otherwise indicated. EDV = end-diastolic volume, NS = not significant.

Figure 6

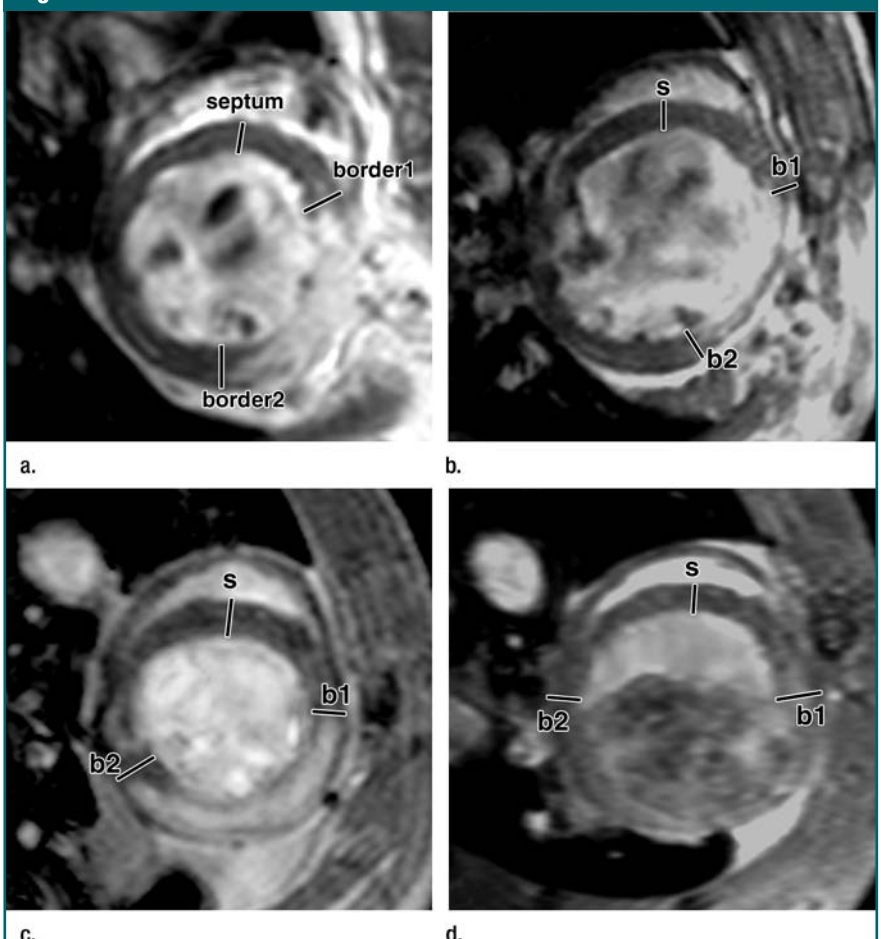

Figure 6: FS of myocardial wall measured from MR images. Short-axis views of **(a, b)** control and **(c, d)** ESC-treated hearts illustrate method of measurement of anterior (border1 *[b1]*) and posterior (border2 *[b2]*) border-zone and septal *(s)* regions for use in quantification of FS. Detailed definitions of border zones are provided in Appendix E1 (*http://radiology.rsnajnls.org/cgi/content/full/250/3/821/DC1*).

Results

Cell viability, iron content, and labeling efficiency are provided in Appendix E1 (*http://radiology.rsnajnls.org/cgi/content/full/250/3/821/DC1*).

ESC Survival and Graft Morphology Detected with PET and MR Imaging

In our pilot study, FHBG signal was detected earlier in rats receiving 5 million cells compared with rats receiving 1 million cells (day 4 vs day 7, Appendix E1 [*http://radiology.rsnajnls.org/cgi/content/full/250/3/821/DC1*]).

In our myocardial ESC infarct study, FHBG signal was shown to localize to the myocardium (Fig 1). Over time, the FHBG signal expanded in this region and increased in intensity, suggesting proliferation of grafted cells. There was also nonspecific FHBG signal in the rib cage and spinal region at an early time, the nature of which was not clear although it has been noted by others (3,4). A trend toward greater (but not significant) percentage of ID per gram was observed in the normal versus infarcted heart at the same dose (Fig 2). FHBG signal was significantly stronger at days 28–30 in rats receiving 5 million cells than it was in those receiving 1 million cells. Fourteen days after injection of 5 million ESCs, the mean end-diastolic myocardial wall thickness in the anterolateral quadrant was 2.8 mm ± 1.5 from group 2, representing an 87% increase compared with a normal mean wall thickness of 1.5 mm ± 0.2 in the anterolateral quadrant, and this quadrant was almost isointense with the neighboring quadrants; however, strong FHBG signal was detected in the corresponding territory, and coregistration demonstrates that the regions containing FHBG signals correspond to the thickened quadrant (Fig 3).

Contributions of Grafted ESCs versus Host Macrophages to the MR Imaging Signal over Time

A distinct hypointense region was observed at day 1 on MR images, and although over time this area became smaller, the residual contrast persisted for at least 4 weeks (Fig 4). The hypoin-

Figure 7

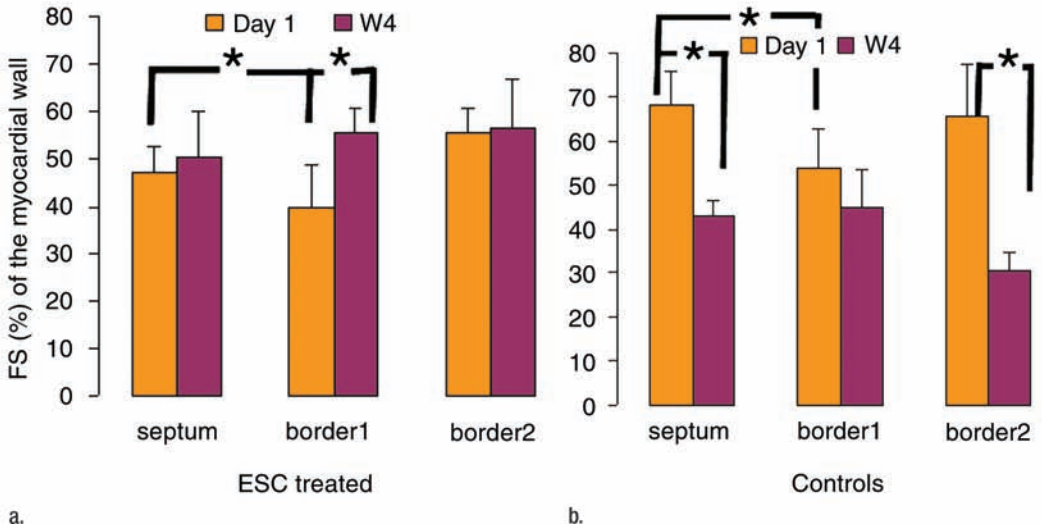

Figure 7: Changes in FS over 4-week time course. **(a, b)** FS in border 1 and 2 and septum regions were plotted from **(a)** ESC-treated and **(b)** control hearts at day 1 and week 4 *(W4)*. $* = P < .05$.

tense territory was significantly smaller at week 4 compared with the hypointense territory at day 1 and was accompanied by a trend of decreasing (not significant) CNR (Fig 5). Histologic analysis revealed that early after injection (4 hours), Prussian blue–positive ESCs, which were small and round with a large nucleus-to-cytoplasm ratio, distributed among cardiac muscle fibers; there were neither free (uninternalized) SPIO labels nor infiltrating macrophages (Fig E6 [*http://radiology.rsnajnls.org/cgi/content/full/250/3/821/DC1*]) at the injection site. At week 4, fewer Prussian blue–positive cells were observed in the graft (teratoma), and the blue signal became aggregated and more intense. In addition, infiltration of host macrophages into the teratoma was revealed by means of positive CD68 staining. Counting of the double-positive cells versus total Prussian blue cells demonstrated that most of the Prussian blue–positive cells were host macrophages (mean, 93% ± 2 in the infarcted hearts and 94% ± 4 in the normal hearts); the rest (≤6%) were CD68 negative.

Assessment of Cardiac Function and Cardiac Differentiation

Mean infarct size determined by using MR imaging was 19.4% ± 4.4 of the LV volume in group 2 and 18.6% ± 6.9 in group 3 ($P = .8$). MR imaging–based quantification of global LV function revealed a reduction in ESV in group 2 at week 4 compared with that at day 1 (ΔESV = −14 μL), whereas an increase in ESV (ΔESV = 117 μL) was found in group 3 ($P < .05$, Table 3). End-diastolic volume was increased in both groups, but the increase was much smaller in group 2 versus 3 ($P < .05$). These changes led to a 12% increase in LV ejection fraction in group 2 versus a 15% reduction in group 3 ($P < .05$). The heart rate decreased in both groups and no difference was found in heart rate between the groups ($P = .49$).

Over the time course of 4 weeks, changes in FS measured at the anterior (border 1) and posterior (border 2) border-zone and remote regions in groups 3 (Fig 6a, 6b) and 2 (Fig 6c, 6d) are summarized in Figure 7. At day 1 in both groups, the FS in border zone 1 significantly decreased compared with the noninfarcted septal regions because of infarction-related events. At week 4 for group 2, FS recovered in border zone 1 ($P < .05$), whereas it was maintained in border zone 2 and in the septum; for group 3, however, FS remained suppressed in border zone 1 and deteriorated in border zone 2 and septal regions ($P < .05$). The teratoma appears to form in the infarcted territory and grow toward the lumen; this growth pattern was confirmed by means of trichrome staining (Fig E2 [*http://radiology.rsnajnls.org/cgi/content/full/250/3/821/DC1*]): Teratoma grew primarily from the infarcted region and penetrated approximately 2 mm into the border zone on both sides, thereby physically linking the residual myocardial wall in the infarcted zone to the border zones. This growth pattern leads to an apparent increase in wall thickness in the infarct region that is observed by using MR imaging.

The prevalence of teratoma formation at week 4 was 100% in both normal and infarcted hearts receiving 1 million or 5 million ESCs. The percentage of cardiomyocytes estimated from cardiac-specific α-actinin staining (Fig E3 [*http://radiology.rsnajnls.org/cgi/content/full/250/3/821/DC1*]) is summarized in Table 4. Less than 0.5% of the cells in teratomas were cardiomyocytes, and although characteristic striations were clearly visualized, these muscle fibers were not well organized. Although no difference in cardiac differentiation was seen between teratomas formed in the normal versus the infarcted hearts, the percentage of cardiomyocytes in the teratoma was inversely dependent on the dose

of ESCs: In hearts injected with 1 million cells, 0.46% cell populations in the teratomas were cardiomyocytes versus 0.27% in hearts injected with 5 million cells ($P < .05$).

Discussion

We demonstrated the feasibility of double labeling ESCs with a PET reporter gene and MR imaging–detectable SPIO particles to evaluate their distribution, survival, and effects on remodeling after MI. We found the following results: *(a)* ESCs can be localized early after injection and their survival and/or proliferation can be followed for at least 4 weeks after MI. *(b)* At week 4, most SPIO labels are contained in infiltrating macrophages, not ESCs. *(c)* Despite teratoma formation, ESC-treated rats have improved global, and preserved regional, LV function as a result of favorable ventricular remodeling after MI, which seems unrelated to the low incidence of cardiac differentiation of ESCs.

SPIO labeling permitted visualization of detailed cell distribution by using MR imaging at day 1, a few days before the FHBG signals became detectable. This information is important to confirm the success of injection and location of cells. The reporter gene, on the other hand, provides an authentic marker of cell survival. The combination of the two allowed the overcoming of a common limitation of current cell labeling methods (ie, label dilution caused by cell proliferation) and led to findings not possible with either technique individually. First, when a significant reduction of the SPIO-related hypointense area occurred between day 1 and week 4, the sharp increase in PET signal revealed rapid proliferation of grafted cells. These data suggested that the reduced hypointense MR imaging signal might be less sensitive in detecting the surviving ESCs because SPIO labels would be substantially diluted in rapidly proliferating cells. Detailed immunohistochemical analysis demonstrated that the majority of Prussian blue–positive cells in the week 4 grafts were host macrophages (via rat-specific CD68 antibodies), confirming that the residual hypointense signal originates from infiltrating macrophages rather than from stem cells that have differentiated into macrophages. Second, in some cases, MR signals from the grafted cells become isointense with the surrounding myocardium. Coregistration permits localization of the surviving cells (FHBG positive) to the anterolateral myocardial wall, which became thicker than normal. The link between the surviving cells and the morphology of the graft formed by these cells is achieved through the dual-modality approach. Without the knowledge of cell survival, abnormal wall thickness could be associated with hypertrophy of residual myocardium stimulated by ESC-secreted growth factors instead of grafts formed by proliferating ESCs.

Our study revealed an increased LV ejection fraction and a preserved FS at week 4 after MI in ESC-treated hearts compared with culture media–treated hearts. However, a lack of contractile function in the teratoma region was revealed by using tagged MR imaging ($n = 4$) (Movie 2 [*http://radiology.rsnajnls.org/cgi/content/full/250/3/821/DC1*]) and is consistent with immunohistochemical analysis results that indicated that less than 0.5% of the cell population in the teratoma represented cardiomyocytes.

Table 4

Percentage of Cardiomyocytes in Teratoma

Statistic	1 Million Cells ($n = 8$)	5 Million Cells ($n = 8$)	Normal Heart ($n = 8$)	Infarcted Heart ($n = 8$)
Mean ± standard deviation	0.46% ± 0.16	0.27% ± 0.10	0.38% ± 0.13	0.37% ± 0.22
P value	<.05*	. . .	NS†	. . .

* For 1 million versus 5 million cells. *P* value represents a significant difference.

† For normal versus infarcted heart. NS = not significant.

In regard to the underlying mechanisms responsible for improvement in cardiac function, it is possible that the presence of any new cells (not necessarily cardiomyocytes) may reduce or redistribute the wall stress in the infarcted and border-zone regions, leading to less unfavorable ventricular remodeling after MI. This hypothesis is supported by the close integration of the teratoma with the myocardial wall observed at trichrome staining. However, a paracrine effect (21) caused by the presence and proliferation of ESCs could not be excluded.

Our study had limitations. First, use of ESCs led to teratoma formation, which limited therapeutic evaluation in a clinically relevant manner. Injection of ESC-derived cardiac progenitor cells rather than undifferentiated ESCs would represent a safer approach for myocardial regeneration (21–23). Second, the potential for SPIO label dilution in rapidly proliferating ESCs (mean doubling time, 23.5 hours ± 5.8) (24) and label association with infiltrating macrophages has been clearly demonstrated in this study. However, whether these properties are applicable to other types of stem cells, which are not as highly proliferative as ESCs, needs further investigation. Third, the protrusion of teratomas into the LV lumen might have contributed to the increased LV ejection fraction seen as a consequence of technical factors in the ejection fraction calculation and may also affect proper delineation of the anterior and posterior border zones. Fourth, we performed PET and MR imaging on consecutive days. A unified PET/MR imager would permit concurrent dual-modality imaging and direct coregistration. Fifth, group 3 did not undergo PET but did undergo MR imaging for comparison of ventricular function with group 2. However, prior data from our laboratory suggest that the nonspecific uptake of the FHBG tracer occurs primarily in the gastrointestinal tract instead of cardiac tissues (25); therefore, this factor was unlikely to affect our results.

In summary, ESCs double labeled with a PET reporter gene and SPIO particles permit serial noninvasive evaluation of stem cell fate by using PET and

MR imaging techniques and have a favorable effect on remodeling after MI. The double-labeling and dual-detection technique is readily translatable to ESC-derived cardiac progenitors and would provide a useful tool to understand the biology and evaluate the potential therapeutic role of these stem cells in clinically relevant cardiac repair.

Acknowledgments: We thank Joel Karp, PhD, Suleman Surti, PhD, and Eric Blankemeyer, BS, for technical assistance with the animal PET scanner and generation of phantom data for calibration of FHBG signals. We thank Bin Huang, MD, for assistance in animal surgery and Richard Freifelder, PhD, for assistance with productions of FHBG tracer. We acknowledge the Small Animal Imaging Facility, University of Pennsylvania, Philadelphia, Pa, for technical assistance and are indebted to Doris A. Taylo r, PhD, University of Minnesota, Minneapolis, Minn, for comments and suggestions.

References

1. Thom T, Haase N, Rosamond W, et al. Heart disease and stroke statistics: 2006 update—a report from the American Heart Association Statistics Committee and Stroke Statistics Subcommittee. Circulation 2006;113:e85–e151. [Published corrections appear in Circulation 2006;113: e696 and 2006;114:e630.]
2. Young JB, Dunlap ME, Pfeffer MA, et al. Mortality and morbidity reduction with Candesartan in patients with chronic heart failure and left ventricular systolic dysfunction: results of the CHARM low-left ventricular ejection fraction trials. Circulation 2004; 110:2618–2626.
3. Wu JC, Chen IY, Sundaresan G, et al. Molecular imaging of cardiac cell transplantation in living animals using optical bioluminescence and positron emission tomography. Circulation 2003;108:1302–1305.
4. Cao F, Lin S, Xie X, et al. In vivo visualization of embryonic stem cell survival, proliferation, and migration after cardiac delivery. Circulation 2006;113:1005–1014.
5. Qiao H, Choi SR, Acton P, Kung H, Ferrari VA, Zhou R. PET imaging of embryonic stem cells grafted in the infarcted myocardium. Presented at the fifth annual meeting of the Society of Molecular Imaging, Hawaii, Hawaii, August 30 to September 2, 2006.
6. Kraitchman DL, Heldman AW, Atalar E, et al. In vivo magnetic resonance imaging of mesenchymal stem cells in myocardial infarction. Circulation 2003;107:2290–2293.
7. Hill JM, Dick AJ, Raman VK, et al. Serial cardiac magnetic resonance imaging of injected mesenchymal stem cells. Circulation 2003;108:1009–1014.
8. Himes N, Min JY, Lee R, et al. In vivo MRI of embryonic stem cells in a mouse model of myocardial infarction. Magn Reson Med 2004;52:1214–1219.
9. Cahill KS, Germain S, Byrne BJ, Walter GA. Non-invasive analysis of myoblast transplants in rodent cardiac muscle. Int J Cardiovasc Imaging 2004;20:593–598.
10. Arai T, Kofidis T, Bulte JW, et al. Dual in vivo magnetic resonance evaluation of magnetically labeled mouse embryonic stem cells and cardiac function at 1.5 t. Magn Reson Med 2006;55:203–209.
11. Tallheden T, Nannmark U, Lorentzon M, et al. In vivo MR imaging of magnetically labeled human embryonic stem cells. Life Sci 2006;79:999–1006.
12. Ebert SN, Taylor DG, Nguyen HL, et al. Noninvasive tracking of cardiac embryonic stem cells in vivo using magnetic resonance imaging techniques. Stem Cells 2007;25:2936–2944.
13. Zhang H, Qiao H, Ponde D, et al. MRI and PET dual detection of embryonic stem cells grafted in the myocardium [abstr]. In: Proceedings of the Fifteenth Meeting of the International Society for Magnetic Resonance in Medicine. Berkeley, Calif: International Society for Magnetic Resonance in Medicine, 2007; 1210.
14. Zhou R, Thomas DH, Qiao H, et al. In vivo detection of stem cells grafted in infarcted rat myocardium. J Nucl Med 2005;46:816–822.
15. Surti S, Karp JS, Perkins AE, Freifelder R, Muehllehner G. Design evaluation of A-PET: a high sensitivity animal PET camera. IEEE Trans Nucl Sci 2003;50:1357–1363.
16. Surti S, Karp JS, Perkins AE, et al. Imaging performance of A-PET: a small animal PET camera. IEEE Trans Med Imaging 2005;24: 844–852.
17. Zhou R, Pickup S, Glickson JD, Scott C, Ferrari VA. Assessment of global and regional myocardial function in the mouse using cine- and tagged MRI. Magn Reson Med 2003;49:760–764.
18. Thomas D, Dumont C, Pickup S, et al. T1-weighted cine FLASH is superior to IR imaging of post-infarction myocardial viability at 4.7T. J Cardiovasc Magn Reson 2006;8:345–352. [Published correction appears in J Cardiovasc Magn Reson 2006;8:683.]
19. Yang Z, Berr SS, Gilson WD, Toufektsian MC, French BA. Simultaneous evaluation of infarct size and cardiac function in intact mice by contrast-enhanced cardiac magnetic resonance imaging reveals contractile dysfunction in noninfarcted regions early after myocardial infarction. Circulation 2004;109: 1161–1167.
20. Lazarous DF, Shou M, Unger EF. Combined bromodeoxyuridine immunohistochemistry and Masson trichrome staining: facilitated detection of cell proliferation in viable vs. infarcted myocardium. Biotech Histochem 1992;67:253–255.
21. Behfar A, Perez-Terzic C, Faustino RS, et al. Cardiopoietic programming of embryonic stem cells for tumor-free heart repair. J Exp Med 2007;204:405–420.
22. Kattman SJ, Adler ED, Keller GM. Specification of multipotential cardiovascular progenitor cells during embryonic stem cell differentiation and embryonic development. Trends Cardiovasc Med 2007;17:240–246.
23. Laflamme MA, Chen KY, Naumova AV, et al. Cardiomyocytes derived from human embryonic stem cells in pro-survival factors enhance function of infarcted rat hearts. Nat Biotechnol 2007;25:1015–1024.
24. Fok EY, Zandstra PW. Shear-controlled single-step mouse embryonic stem cell expansion and embryoid body-based differentiation. Stem Cells 2005;23:1333–1342.
25. Acton PD, Zhou R. Imaging reporter genes for cell tracking with PET and SPECT. Q J Nucl Med Mol Imaging 2005;49:349–360.

Radiology 2009

This is your reprint order form or pro forma invoice

(Please keep a copy of this document for your records.)

Reprint order forms and purchase orders or prepayments must be received 72 hours after receipt of form either by mail or by fax at 410-820-9765. It is the policy of Cadmus Reprints to issue one invoice per order. **Please print clearly**.

Author Name _____
Title of Article _____
Issue of Journal_____ Reprint # _____ Publication Date _____
Number of Pages_____ KB # _____ Symbol Radiology
Color in Article? Yes / No (Please Circle)

Please include the journal name and reprint number or manuscript number on your purchase order or other correspondence.

Order and Shipping Information

Reprint Costs **(Please see page 2 of 2 for reprint costs/fees.)**

_____ Number of reprints ordered $_____
_____ Number of color reprints ordered $_____
_____ Number of covers ordered $_____
Subtotal $_____
Taxes $_____

(*Add appropriate sales tax for Virginia, Maryland, Pennsylvania, and the District of Columbia or Canadian GST to the reprints if your order is to be shipped to these locations*.)

First address included, add $32 for each additional shipping address $_____

TOTAL $_____

Shipping Address **(cannot ship to a P.O. Box) Please Print Clearly**

Name _____
Institution _____
Street _____
City _____ State _____ Zip _____
Country _____
Quantity_____ Fax _____
Phone: Day _____ Evening _____
E-mail Address _____

Additional Shipping Address* **(cannot ship to a P.O. Box)**

Name _____
Institution _____
Street _____
City _____ State _____ Zip _____
Country _____
Quantity _____ Fax _____
Phone: Day _____ Evening _____
E-mail Address _____

** Add $32 for each additional shipping address*

Payment and Credit Card Details

Enclosed: Personal Check _____
Credit Card Payment Details _____

Checks must be paid in U.S. dollars and drawn on a U.S. Bank.

Credit Card: __ VISA __ Am. Exp. __ MasterCard
Card Number _____
Expiration Date_____
Signature: _____

Please send your order form and prepayment made payable to:

Cadmus Reprints
P.O. Box 751903
Charlotte, NC 28275-1903

Note: Do not send express packages to this location, PO Box.

FEIN #:541274108

Invoice or Credit Card Information

Invoice Address **Please Print Clearly**

Please complete Invoice address as it appears on credit card statement

Name _____
Institution _____
Department _____
Street _____
City _____ State _____ Zip _____
Country _____
Phone _____ Fax _____
E-mail Address _____

Cadmus will process credit cards and *Cadmus Journal Services* will appear on the credit card statement.

If you don't mail your order form, you may fax it to 410-820-9765 with your credit card information.

Signature _____ Date _____

Signature is required. By signing this form, the author agrees to accept the responsibility for the payment of reprints and/or all charges described in this document.

RB-1/01/09

Radiology 2009

Black and White Reprint Prices

Domestic (USA only)						
# of Pages	50	100	200	300	400	500
1-4	$239	$260	$285	$303	$323	$340
5-8	$379	$420	$455	$491	$534	$572
9-12	$507	$560	$651	$684	$748	$814
13-16	$627	$698	$784	$868	$954	$1,038
17-20	$755	$845	$947	$1,064	$1,166	$1,272
21-24	$878	$985	$1,115	$1,250	$1,377	$1,518
25-28	$1,003	$1,136	$1,294	$1,446	$1,607	$1,757
29-32	$1,128	$1,281	$1,459	$1,632	$1,819	$2,002
Covers	$149	$164	$219	$275	$335	$393

International (includes Canada and Mexico)						
# of Pages	50	100	200	300	400	500
1-4	$299	$314	$367	$429	$484	$546
5-8	$470	$502	$616	$722	$838	$949
9-12	$637	$687	$852	$1,031	$1,190	$1,369
13-16	$794	$861	$1,088	$1,313	$1,540	$1,765
17-20	$963	$1,051	$1,324	$1,619	$1,892	$2,168
21-24	$1,114	$1,222	$1,560	$1,906	$2,244	$2,588
25-28	$1,287	$1,412	$1,801	$2,198	$2,607	$2,998
29-32	$1,441	$1,586	$2,045	$2,499	$2,959	$3,418
Covers	$211	$224	$324	$444	$558	$672

Color Reprint Prices

Domestic (USA only)						
# of Pages	50	100	200	300	400	500
1-4	$247	$267	$385	$515	$650	$780
5-8	$297	$435	$655	$923	$1194	$1467
9-12	$445	$563	$926	$1,339	$1,748	$2,162
13-16	$587	$710	$1,201	$1,748	$2,297	$2,843
17-20	$738	$858	$1,474	$2,167	$2,846	$3,532
21-24	$888	$1,005	$1,750	$2,575	$3,400	$4,230
25-28	$1,035	$1,164	$2,034	$2,986	$3,957	$4,912
29-32	$1,186	$1,311	$2,302	$3,402	$4,509	$5,612
Covers	$149	$164	$219	$275	$335	$393

International (includes Canada and Mexico))						
# of Pages	50	100	200	300	400	500
1-4	$306	$321	$467	$642	$811	$986
5-8	$387	$517	$816	$1,154	$1,498	$1,844
9-12	$574	$689	$1,157	$1,686	$2,190	$2,717
13-16	$754	$874	$1,506	$2,193	$2,883	$3,570
17-20	$710	$1,063	$1,852	$2,722	$3,572	$4,428
21-24	$1,124	$1,242	$2,195	$3,231	$4,267	$5,300
25-28	$1,320	$1,440	$2,541	$3,738	$4,957	$6,153
29-32	$1,498	$1,616	$2,888	$4,269	$5,649	$7028
Covers	$211	$224	$324	$444	$558	$672

Minimum order is 50 copies. For orders larger than 500 copies, please consult Cadmus Reprints at 800-407-9190.

Reprint Cover

Cover prices are listed above. The cover will include the publication title, article title, and author name in black.

Shipping

Shipping costs are included in the reprint prices. Domestic orders are shipped via FedEx Ground service. Foreign orders are shipped via a proof of delivery air service.

Multiple Shipments

Orders can be shipped to more than one location. Please be aware that it will cost $32 for each additional location.

Delivery

Your order will be shipped within 2 weeks of the journal print date. Allow extra time for delivery.

Tax Due

Residents of Virginia, Maryland, Pennsylvania, and the District of Columbia are required to add the appropriate sales tax to each reprint order. For orders shipped to Canada, please add 7% Canadian GST unless exemption is claimed.

Ordering

Reprint order forms and purchase order or prepayment is required to process your order. Please reference journal name and reprint number or manuscript number on any correspondence. You may use the reverse side of this form as a proforma invoice. Please return your order form and prepayment to:

Cadmus Reprints
P.O. Box 751903
Charlotte, NC 28275-1903

Note: Do not send express packages to this location, PO Box.
FEIN #:541274108

Please direct all inquiries to:

Rose A. Baynard
800-407-9190 (toll free number)
410-819-3966 (direct number)
410-820-9765 (FAX number)
baynardr@cadmus.com (e-mail)

Reprint Order Forms and purchase order or prepayments must be received 72 hours after receipt of form.